ORIGINAL ARTICLE

Respiratory Syncytial Virus Infection Promotes Necroptosis and HMGB1 Release by Airway Epithelial Cells

Jennifer Simpson[1,2], Zhixuan Loh[2], Md Ashik Ullah[1,2], Jason P. Lynch[1,2], Rhiannon B. Werder[1,2], Natasha Collinson[1], Vivian Zhang[1,2], Yves Dondelinger[3,4], Mathieu J. M. Bertrand[3,4], Mark L. Everard[5], Christopher C. Blyth[5,6,7,8], Gunter Hartel[1], Antoon J. Van Oosterhout[9], Peter J. Gough[10], John Bertin[10], John W. Upham[11,12], Kirsten M. Spann[13]*, and Simon Phipps[1,2,12]*

[1]QIMR Berghofer Medical Research Institute, Herston, Australia; [2]School of Biomedical Science, University of Queensland, Brisbane, Queensland, Australia; [3]VIB Center for Inflammation Research, Ghent, Belgium; [4]Department of Biomedical Molecular Biology, Ghent University, Ghent, Belgium; [5]School of Medicine and [8]Wesfarmers Centre for Vaccines and Infectious Diseases, Telethon Kids Institute, University of Western Australia, Perth, Western Australia, Australia; [6]Department of Infectious Diseases, Perth Children's Hospital, Perth, Western Australia, Australia; [7]Department of Microbiology, PathWest Laboratory Medicine WA, QEII Medical Centre, Perth, Western Australia, Australia; [9]GlaxoSmithKline, Stevenage, United Kingdom; [10]GlaxoSmithKline, Philadelphia, Pennsylvania; [11]University of Queensland Diamantina Institute, Brisbane, Queensland, Australia; [12]Australian Infectious Diseases Research Centre, Brisbane, Queensland, Australia; and [13]Queensland University of Technology, Brisbane, Queensland, Australia

Abstract

Rationale: Respiratory syncytial virus (RSV) bronchiolitis causes significant infant mortality. Bronchiolitis is characterized by airway epithelial cell (AEC) death; however, the mode of death remains unknown.

Objectives: To determine whether necroptosis contributes to RSV bronchiolitis pathogenesis via HMGB1 (high mobility group box 1) release.

Methods: Nasopharyngeal samples were collected from children presenting to the hospital with acute respiratory infection. Primary human AECs and neonatal mice were inoculated with RSV and murine *Pneumovirus*, respectively. Necroptosis was determined via viability assays and immunohistochemistry for RIPK1 (receptor-interacting protein kinase-1), MLKL (mixed lineage kinase domain-like pseudokinase) protein, and caspase-3. Necroptosis was blocked using pharmacological inhibitors and RIPK1 kinase-dead knockin mice.

Measurements and Main Results: HMGB1 levels were elevated in nasopharyngeal samples of children with acute RSV infection. RSV-induced epithelial cell death was associated with increased phosphorylated RIPK1 and phosphorylated MLKL but not active caspase-3 expression. Inhibition of RIPK1 or MLKL attenuated RSV-induced HMGB1 translocation and release, and lowered viral load. MLKL inhibition increased active caspase-3 expression in a caspase-8/9–dependent manner. In susceptible mice, *Pneumovirus* infection upregulated RIPK1 and MLKL expression in the airway epithelium at 8 to 10 days after infection, coinciding with AEC sloughing, HMGB1 release, and neutrophilic inflammation. Genetic or pharmacological inhibition of RIPK1 or MLKL attenuated these pathologies, lowered viral load, and prevented type 2 inflammation and airway remodeling. Necroptosis inhibition in early life ameliorated asthma progression induced by viral or allergen challenge in later life.

Conclusions: *Pneumovirus* infection induces AEC necroptosis. Inhibition of necroptosis may be a viable strategy to limit the severity of viral bronchiolitis and break its nexus with asthma.

Keywords: bronchiolitis; asthma; MLKL; *Pneumovirus*; necroptosis

(Received in original form June 9, 2019; accepted in final form February 26, 2020)

*These authors contributed equally to this work.

Supported by ARC Australia (S.P.), NHMRC Australia (S.P.), GlaxoSmithKline (S.P.), and Fonds voor Wetenschappelijk Onderzoek Vlaanderen (M.J.M.B. and Y.D.).

Author Contributions: A.J.V.O. and S.P. conceived the idea for the project. J.S. and S.P. designed the experiments. J.S., K.M.S., and S.P. interpreted the data and wrote the first draft of the manuscript, and all remaining authors edited to generate the final version. J.S., Z.L., M.A.U., J.P.L., R.B.W., N.C., and V.Z. performed the experiments. Y.D., M.J.M.B., M.L.E., C.C.B., G.H., A.J.V.O., P.J.G., J.B., J.W.U., and K.M.S. provided intellectual input and reagents.

Correspondence and requests for reprints should be addressed to Simon Phipps, Ph.D., 300 Herston Road, Herston QLD 4006, Australia. E-mail: simon.phipps@qimrberghofer.edu.au.

This article has a related editorial.

This article has an online supplement, which is accessible from this issue's table of contents at www.atsjournals.org.

Am J Respir Crit Care Med Vol 201, Iss 11, pp 1358–1371, Jun 1, 2020

Originally Published in Press as DOI: 10.1164/rccm.201906-1149OC on February 27, 2020
Internet address: www.atsjournals.org

At a Glance Commentary

Scientific Knowledge on the Subject: Respiratory syncytial virus (RSV)-associated bronchiolitis is a significant cause of global mortality and morbidity. Additionally, severe bronchiolitis in infancy is a risk factor for childhood asthma. Currently, there is no approved vaccine for RSV, and therefore novel therapeutics are required. Airway epithelial death and sloughing is a common pathology associated with RSV bronchiolitis and is typically viewed as a beneficial response to limit viral spread. However, the mode of cell death, now recognized to profoundly influence host immunity, and hence health outcomes, remains unclear.

What This Study Adds to the Field: This study is the first to show that RSV infection induces a mode of programmed cell death, termed necroptosis. Inhibition of the necroptosis-associated proteins pRIPK1 (phosphorylated receptor-interacting protein kinase-1) and MLKL (mixed lineage kinase domain-like pseudokinase) ameliorated viral bronchiolitis–associated pathologies in mice and prevented the later progression to asthma. At the molecular level, in both human primary bronchial epithelial cells and susceptible mice, blockade of necroptosis attenuated the release of the nuclear alarmin HMGB1 (high mobility group box 1), lowered viral load, and prevented the onset of type-2 inflammation. Inhibition of necroptosis may be a viable strategy to limit the severity of viral bronchiolitis and break its nexus with asthma.

Respiratory syncytial virus (RSV)-induced bronchiolitis is associated with significant mortality worldwide (1). Additionally, severe RSV bronchiolitis in infancy is associated with subsequent airways disease, including asthma (2–4). In the absence of an approved vaccine for RSV, new treatments that effectively manage and reduce RSV-associated pathogenesis are urgently needed. Pathologically, severe bronchiolitis is characterized by neutrophilic inflammation, mucus hypersecretion, and airway epithelial cell (AEC) sloughing (5, 6). These dead epithelial cells, together with a viscous exudate, can form dense plugs in the bronchiolar lumen that impede breathing (6, 7). Despite this, the prevailing view is that AEC death is a beneficial defense mechanism, limiting viral spread.

Host defense to viral infection depends on the activation of innate pattern recognition receptors, which induce the production of antiviral cytokines such as type I and III IFNs. In turn, these cytokines initiate the antiviral state to restrict virus replication and spread, and promote the activation of natural killer cells and cytotoxic T lymphocytes that ultimately clear the virus by inducing apoptotic death of infected cells (8). Genetic and/or environmental factors that perturb the successful coordination of this response predispose toward severe RSV bronchiolitis (9–11). To model the immunopathology and sequelae, we developed a preclinical gene–environment model by inoculating IRF7 (IFN regulatory factor 7)-deficient mice with pneumonia virus of mice (PVM), a mouse *Pneumovirus* and homolog of RSV. As a consequence of impaired antiviral immunity, these mice develop severe epithelial sloughing, leading to HMGB1 (high mobility group box 1) release and neutrophilic inflammation in early life, and they are predisposed to asthma in later life. Critically, HMGB1 neutralization ablated all of these events (unpublished observations).

HMGB1 is a chromatin-binding protein that can be released into the extracellular space to function as a proinflammatory cytokine. As a consequence, its release and activation state is highly controlled. Cellular mechanisms known to regulate HMGB1 release include vesicular transport, inflammasome activation, necrosis, and necroptosis (12–15). This recently identified form of programmed cell death is initiated by the formation of a multiprotein complex termed the necrosome (16), which typically contains pRIPK1 (phosphorylated receptor-interacting protein kinase-1) (phosphorylated [p]S166) and pRIPK3, leading to the phosphorylation of MLKL (mixed lineage kinase domain-like pseudokinase) (13, 14, 17, 18). In contrast to apoptosis, necroptosis most commonly elicits a proinflammatory response, in keeping with its role in mediating HMGB1 release, and can delay viral clearance (19). This led us to question the current dogma that the induction of AEC death during RSV bronchiolitis serves to restrict virus spread and limit host immunopathology. Specifically, we interrogated the mode of RSV-associated AEC death and downstream HMGB1 release using primary human AECs (hAECs) and mouse AECs (mAECs) in culture. To support our *in vitro* findings, we evaluated the mechanism of AEC sloughing and HMGB1 release, and the effect of necroptosis inhibition, in our preclinical model of severe viral bronchiolitis and later experimental asthma.

Methods

Human Subjects and Nasopharyngeal Samples

Samples were prospectively collected from 2-year-old children (interquartile range, 1.25–3.86) presenting with acute respiratory infection to the Princess Margaret Hospital, Perth, Australia. Ethical approval was obtained from the ethics committees of Princess Margaret Hospital for Children (ethics identification number 1,673/EP), the South Metropolitan Area Health Service, and the Western Australian Aboriginal Health Information and Ethics Committee. All samples were frozen at −80°C before the measurement of HMGB1 by ELISA (Chondrex). The presence of respiratory viruses was tested by PCR assay.

hAEC Culture and Treatment

hAECs from healthy pediatric (age 2–3 yr) donors (Lonza IDs 28195, 28563, 28385, and 29055) were obtained commercially (Lonza). Purified RSV A2 stocks were prepared as previously described (20). Nondifferentiated (submerged) or air–liquid interface (ALI)- differentiated AECs were grown and infected with RSV, as previously described (21, 22). One hour before RSV infection, the cells were pretreated with a pRIPK1 inhibitor (Necrostatin-1s [Nec-1s], 2.2 μM; Biovision) (23), which reduces RIPK1 phosphorylation; an MLKL inhibitor (necrosulfonamide [NSA], 10 μM; Merck) (24), which prevents MLKL translocation to the plasma membrane; a caspase-9 inhibitor (Z-LEHD-FMK, 2 μM; Biovision); and/or a caspase-8 inhibitor

(Z-IETD-FMK, 2 μM; Biovision). After 12 or 24 hours, supernatant was collected and stored at −80°C, and the cells fixed with neutral buffered 10% formalin solution (Sigma) for 15 minutes.

Murine AEC Culture

Murine AECs were cultured as described (21, 25). The cells were inoculated with PVM (multiplicity of infection [MOI] of 0.5) or vehicle, then fixed with formalin 8 hours later. In some experiments, cells were pretreated for 30 minutes with GW806742X (2 μM; SYNkinase) (26) or the RIPK1 inhibitor GSK'963 (4.3 mM; GSK) (27).

Mouse Strains and Treatments

All studies were approved by the University of Queensland and QIMR Berghofer Animal Care and Ethics Committees. $RIPK1^{K45A/K45A}$ mice (GlaxoSmithKline) and $IRF7^{-/-}$ mice (provided by Dr. Tadatsugu Taniguchi, University of Tokyo), were rederived and crossed to generate $IRF7^{-/-}$ $RIPK1^{K45A/K45A}$. Wild-type (WT), $IRF7^{-/-}$, $RIPK1^{K45A/K45A}$, and $IRF7^{-/-}$ $RIPK1^{K45A/K45A}$ mice (all C57BL/6 background) were bred in specific pathogen-free animal houses at the University of Queensland and at QIMR Berghofer. At postnatal Day 7, neonatal mice were inoculated (intranasal route) with 2 plaque-forming units (PFUs) of PVM (J3666 strain) in 10 μl of vehicle (10% fetal calf serum in Dulbecco's Modified Eagle Medium media), as described previously (21). In some experiments, the mice were reinoculated with 100 PFU of PVM at 42 days postinfection (dpi) or given 4 weekly inoculations of 1 μg of cockroach allergen extract (CRE; GREER) commencing at 42 dpi. Control mice received vehicle alone. To inhibit necroptosis, WT and $IRF7^{-/-}$ neonatal mice were injected (i.p. route) with Nec-1s (6 mg/kg at 5 and 7 dpi; Biovision) (23), GSK'963 (10 mg/kg, twice daily from 5 dpi; GSK) (27), or GW806742X (GW80, 50 μg/kg at 7 and 9 dpi; SYNkinase). For analyses at 7 dpi, mice were treated with GW80 at 5 dpi. BAL fluid collection occurred as described previously (28).

BAL fluid collection, flow cytometry, cytokine analysis, immunohistochemistry and immunofluorescence, quantitative real-time PCR, and ALI culture and treatment details are provided in the online supplement.

Statistical Analysis

Statistical analyses were performed using GraphPad Prism v.6.0 and JMP Pro (v 15.0; SAS Institute). Student's *t* test or the Mann-Whitney *t* test were used for comparing two groups. When more than two groups were compared, data were analyzed using a one-way or two-way ANOVA with Dunnett's or Sidak's *post hoc* test to compare with a control group, respectively. The specific procedure is annotated for Figures 1–8. Although our decision to use parametric analyses is based on longer-term experience with the specific assays producing normal residuals (29), we examined the residuals ($n \geq 16$) from each analysis for normality using the Shapiro-Wilks test and normal quantile plots as a quality control measure. In all but one case, normality was supported. In Figure 2C there was one outlier in the RSV condition, which, when excluded, yielded approximate normality. The results for this analysis were similar whether the outlier was excluded or not, or using robust alternatives (Kruskal-Wallis test with Dunn's *post hoc* test). All analyses involving the four human donor samples were also reanalyzed using mixed-effects models with donor as a random effect.

Differences in HMGB1 expression in nasopharyngeal samples were analyzed using a Mann-Whitney *t* test because this assay tends to generate skewed data. We annotated statistically significant results with * or #, $P < 0.05$; ** or ##, $P < 0.01$; and *** or ###, $P < 0.001$.

Results

RSV Infection of Primary hAECs Activates RIPK1 and MLKL

To address whether RSV infection is associated with increased levels of HMGB1, we obtained nasopharyngeal samples from young children presenting to hospital with acute respiratory infection. HMGB1 levels were significantly greater in the children infected with RSV compared with an infection with a different respiratory virus (Figure 1A). We then obtained primary hAECs from healthy children to assess mechanisms of HMGB1 release *in vitro* (30). RSV (MOI 1) significantly increased nuclear-to-cytoplasmic translocation of HMGB1 and extracellular HMGB1 release at 24 hours postinfection (hpi; *see* Figures 1B and 1C). This was associated with elevated release of double-stranded (ds)DNA and lactate dehydrogenase (LDH), and loss of plasma membrane integrity, shown by increased propidium iodide staining, all indicative of cell death (*see* Figure 1D). To explore the mode of cell death, we stained the AECs for active (cleaved) caspase-3 (CC3), annexin V, pRIPK1 (Ser166), and pMLKL (phosphorylated MLKL) (Ser358). The negative immunoreactivity for CC3 and annexin V and positive immunoreactivity for pRIPK1 and pMLKL suggested the cells were undergoing necroptosis, not apoptosis (*see* Figures 1E–1G). These data were reanalyzed using random-effects models to account for possible donor effects. These analyses yielded the same conclusions, and donor effects were not substantial or significant (data not shown).

Pharmacological Inhibition of RIPK1 or MLKL Attenuates RSV-induced HMGB1 Release

To assess whether necroptosis actively contributes to RSV-induced HMGB1 release at 24 hpi, we treated hAECs with Nec-1s or NSA to inhibit RIPK1 and MLKL, respectively (31, 32). Nec-1s treatment significantly decreased $pRIPK1^+$ and $pMLKL^+$ cells, whereas NSA, acting downstream of pRIPK1, significantly decreased the fraction of $pMLKL^+$ cells (*see* Figure 2A). The MLKL inhibitor increased $CC3^+$ cells (*see* Figure 2A, bottom right panel) and annexin V^+ cells (*see* Figure 2B). Increased CC3 expression was ablated when both caspase-8 and 9 were inhibited, suggesting both intrinsic and extrinsic apoptosis pathways are induced upon MLKL inhibition (*see* Figure E1A in the online supplement). RIPK1 or MLKL inhibition significantly decreased translocation and release of HMGB1 (*see* Figures 2C and 2D), and lowered viral load (*see* Figures 2E and E1B). Simultaneous inhibition of MLKL, caspase-8 and caspase-9 attenuated this protective effect, implicating a role for both intrinsic and extrinsic apoptosis pathways in viral clearance (*see* Figure E1A). Lower viral burden after MLKL inhibition was not associated with increased type I or type III IFN expression (*see* Figure E1C–E1E). These phenotypes were replicated in ALI-differentiated AECs (*see* Figure E2). Collectively, these data suggest that necroptosis contributes to HMGB1 release and viral persistence.

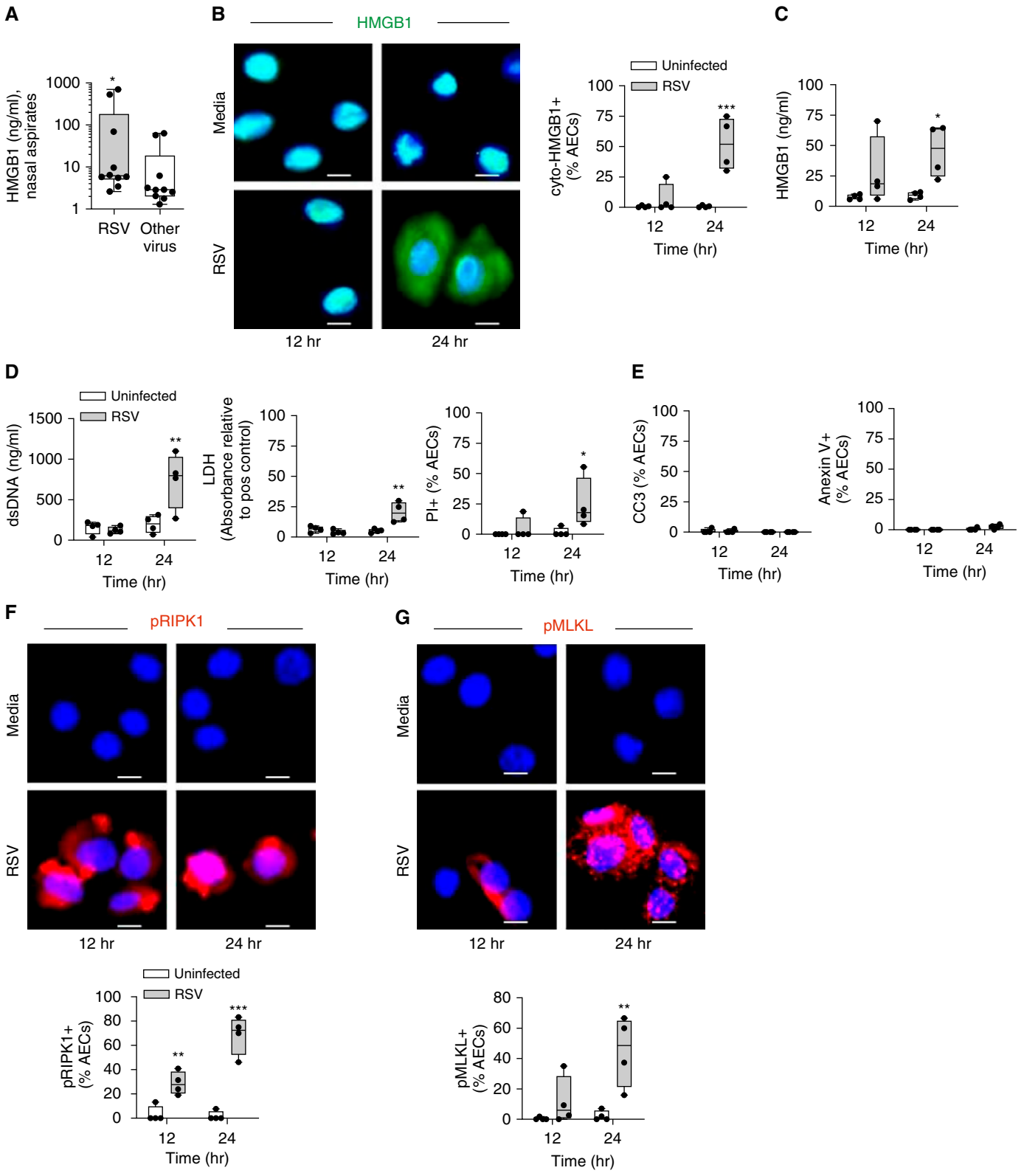

Figure 1. Respiratory syncytial virus (RSV) infection of primary human airway epithelial cells (hAECs) activates RIPK1 (receptor-interacting protein kinase-1) and MLKL (mixed lineage kinase domain-like pseudokinase). (*A*) HMGB1 (high mobility group box 1) levels assessed in nasopharyngeal samples obtained from young children presenting with acute respiratory infection with RSV or other respiratory viruses. (*B–G*) Submerged primary hAECs were infected with RSV (multiplicity of infection of 1), and HMGB1 expression and various analyses of cell death were examined at 12 and 24 hours. (*B*)

Pneumovirus Infection Induces Necroptotic Cell Death in the Airway Epithelium *In Vivo*

We next sought to determine whether necroptosis is pathogenic in a high-fidelity preclinical model of viral bronchiolitis. As a natural mouse pathogen, PVM can be administered at low doses, allowing for the study of host–pathogen interactions as the virus replicates (21, 28, 33–36). We previously demonstrated that PVM infection of IRF7$^{-/-}$ mice leads to severe viral bronchiolitis, with peak viral burden occurring at 7 dpi, followed by neutrophilic inflammation, extensive epithelial sloughing, and elevated HMGB1 levels in the airway lumen at 10 and 14 dpi (unpublished observations). Because epithelial sloughing is indicative of cell death and necroptosis has been linked to HMGB1 release (12, 37), we first sought to determine the temporal pattern of gene and protein expression for cell death–associated caspases and kinases. At the gene level, using whole lung samples, we did not detect a significant increase in *caspase-3* expression in either the WT or IRF7$^{-/-}$ mice following PVM infection (Figure 3A). In contrast, there was a significant increase in *RIPK1*, *MLKL*, and *RIPK3* gene expression in IRF7$^{-/-}$ compared with WT littermates (*see* Figure 3A). A similar phenotype was observed regarding protein expression: pRIPK1 (Ser166) and MLKL expression was elevated in the airway epithelium at 8, 9, and 10 dpi (*see* Figure 3B). This was associated with elevated levels of dsDNA, LDH, and TNFα (tumor necrosis factor-α) in the airway lumen (*see* Figure E3A). MLKL expression colocalized with pRIPK1 in AECs (*see* Figure 3B) was typically expressed in cells with an abnormal (diffusely stained) nuclei (*see* Figure E3B) and was predominantly observed at the apical surface (*see* Figure E3C), consistent with other reports (38). Moreover, we observed MLKL immunoreactivity in sloughed AECs in the airway lumen, suggesting a link between necroptosis and epithelial denudation (*see* Figure E3D). PVM *SH* gene and PVM protein levels were greater in IRF7$^{-/-}$ compared with WT mice, and peaked at 4 and 7 dpi, respectively (*see* Figure 3C), the period of necroptosis onset (*see* Figure 3B). At both 7 and 10 dpi, the majority of MLKL^{+} AECs were immunoreactive for PVM (*see* Figure E3E). Notably, increasing the viral inoculum to 100 PFU in WT mice increased the fraction of pRIPK1/MLKL^{+} AECs to similar levels as observed in IRF7$^{-/-}$ mice infected with 2 PFU (*see* Figure E3F), suggesting that necroptosis is influenced by viral load and can occur in immunocompetent mice. Collectively, these data suggest that *Pneumovirus* infection leads to necroptosis and that this is heightened when innate antiviral immunity is impaired.

Pharmacological Inhibition of RIPK1 or MLKL Decreases Bronchiolitis-associated Immunopathology

To evaluate whether necroptosis contributes to the pathogenesis of acute bronchiolitis, we treated WT and IRF7$^{-/-}$ mice with the RIPK1 inhibitor, Nec-1s, or the MLKL inhibitor, GW80 (NSA does not inhibit murine MLKL), starting at 5 dpi (Figure 4A). Pharmacological inhibition of RIPK1 or MLKL significantly decreased the fraction of pRIPK1 and MLKL-positive AECs at 10 dpi in the IRF7$^{-/-}$-infected mice. Inhibition of MLKL, but not RIPK1, increased the number of CC3s expressing AECs (*see* Figures 4B and 4C), suggesting a switch in cell death modality. Treatment with either inhibitor significantly decreased viral burden (7 dpi; *see* Figure 4D), an effect that was not related to changes in IFN-α/β/λ expression (data not shown) and ameliorated neutrophilic inflammation (*see* Figure 4E). This was associated with a decrease in epithelial sloughing, as well as LDH and dsDNA but not TNFα expression (10 dpi; *see* Figures 4E and 4F and E4A). RIPK1 or MLKL inhibition was associated with reduced cytoplasmic-HMGB1 + AECs and extracellular HMGB1 (*see* Figure 4G), whereas only MLKL inhibition decreased IL-33 levels in the airway lumen (*see* Figures E4B), suggesting that the pRIPK1/MLKL necrosome regulates epithelial cell death and subsequent HMGB1 release during acute *Pneumovirus* infection *in vivo*.

RIPK1 or MLKL Inhibition Prevents the Development of Type 2 Inflammation

We next assessed the effect of Nec-1s or GW80 treatment on the induction of type 2 inflammation in PVM-infected IRF7$^{-/-}$ mice. Similar to our previous findings in other immunocompromised mice (35, 36), IL-13–producing group 2 innate lymphoid cells, eosinophilic inflammation, airway smooth muscle (ASM) remodeling, and mucus hypersecretion were all elevated in IRF7$^{-/-}$ compared with WT mice (Figure 5). This type 2 inflammatory response was significantly attenuated following treatment with Nec-1s or GW80 (*see* Figure 5). These findings were validated when mice were treated with GSK'963 (*see* Figure E5), another inhibitor of RIPK1 (39), further implicating a role for necroptosis in promoting *Pneumovirus*-associated type 2 inflammation.

RIPK1 Kinase-Dead Knockin Mice Are Protected from Viral Bronchiolitis

Because pharmacological inhibitors can elicit off-target effects, we sought to confirm our findings using RIPK1$^{K45A/K45A}$ transgenic mice in which the scaffold function of RIPK1 is preserved and the kinase activity of RIPK1 is ablated (40). As expected, pRIPK1 and MLKL expression was attenuated in PVM-infected IRF7$^{-/-}$ RIPK1$^{K45A/K45A}$ Tg mice compared with IRF7$^{-/-}$ littermate controls (Figure 6A). Genetic inactivation of RIPK1 enzymatic activity conferred protection against severe viral bronchiolitis (high viral load, neutrophilic inflammation, and AEC sloughing; *see* Figures 6B and 6C), alarmin release (HMGB1; *see* Figure 6D), type 2 inflammation (IL-13–producing group 2 innate lymphoid cells and eosinophils; *see*

Figure 1. (*Continued*). Representative micrographs (×400 magnification; scale bar, 10 μm) of HMGB1 (green) in AECs and quantification of cyto-HMGB1. (*C*) Protein expression of HMGB1 in supernatant. (*D*) Expression of double-stranded (ds)DNA and lactate dehydrogenase (LDH) in supernatant, and quantification of PI^{+} AECs. (*E*) Quantification of cleaved caspase-3 and annexin V^{+} AECs. (*F*) Representative micrographs (×400 magnification; scale bar, 10 μm) of pRIPK1 (phosphorylated RIPK1) (red) in AECs and quantification of pRIPK1^{+} AECs. (*G*) Representative micrographs (×400 magnification; scale bar, 10 μm) of pMLKL (phosphorylated MLKL) (red) in AECs and quantification of pMLKL^{+} AECs. Data are representative of $n = 2$ experiments with four donors in each group and are presented as box-and-whisker plots showing quartiles (boxes) and range (whiskers). (*A–G*) Data were analyzed using Mann-Whitney *t* test (*A*) or two-way ANOVA with Sidak's *post hoc* test (*B–G*). $^{*}P < 0.05$, $^{**}P < 0.01$, and $^{***}P < 0.001$ denote significance between infected and uninfected hAECs at each time point. CC3 = cleaved caspase-3; PI = propidium iodide; pos = positive.

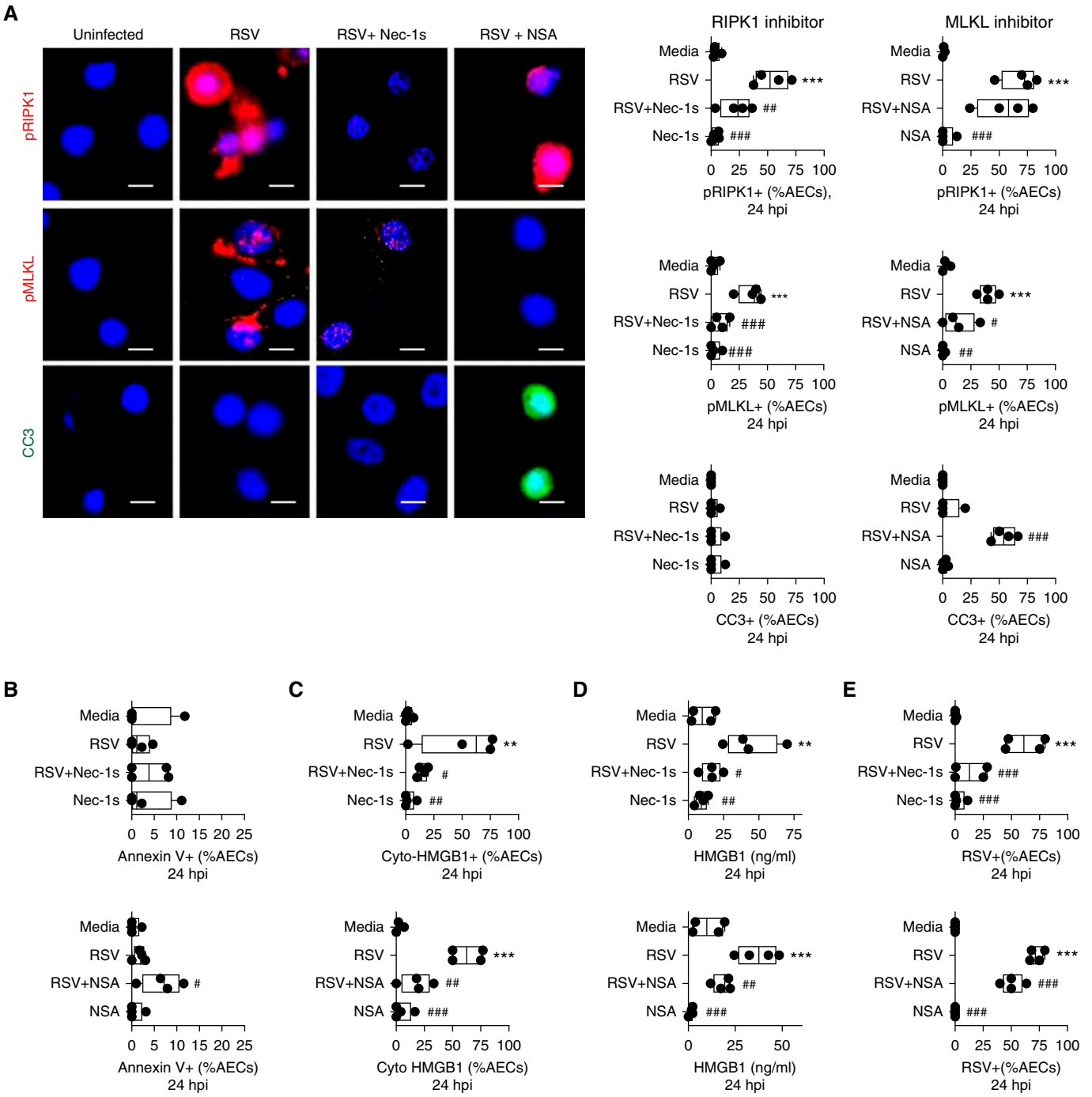

Figure 2. Pharmacological inhibition of RIPK1 (receptor-interacting protein kinase-1) or MLKL (mixed lineage kinase domain-like pseudokinase) attenuates respiratory syncytial virus (RSV)-induced HMGB1 (high mobility group box 1) release. Submerged human airway epithelial cells (hAECs) were pretreated with an RIPK1 inhibitor (Nec-1s) or MLKL inhibitor (NSA) before infection with RSV (multiplicity of infection of 1). (*A*) Representative micrographs (×400 magnification; scale bar, 10 μm) of pRIPK1 (phosphorylated RIPK1) (red); and pMLKL (phosphorylated MLKL) (red) and cleaved caspase-3 (green); and quantification of pRIPK1, pMLKL, and $CC3^+$ AECs. (*B*) Quantification of annexin V^+ AECs. (*C*) Quantification of cyto-$HMGB1^+$ AECs. (*D*) HMGB1 protein expression in supernatant. (*E*) Quantification of RSV^+ AECs. Data are representative of $n = 2$ experiments with four donors in each group and are presented as box-and-whisker plots showing quartiles (boxes) and range (whiskers). Data were analyzed by one-way ANOVA with Dunnett's *post hoc* test. $^{**}P < 0.01$ and $^{***}P < 0.001$ are compared with uninfected hAECs, and $^{\#}P < 0.05$, $^{\#\#}P < 0.01$, and $^{\#\#\#}P < 0.001$ are compared with RSV-infected hAECs. CC3 = cleaved caspase-3; hpi = hours postinfection; Nec-1s = Necrostatin-1s; NSA = necrosulfonamide.

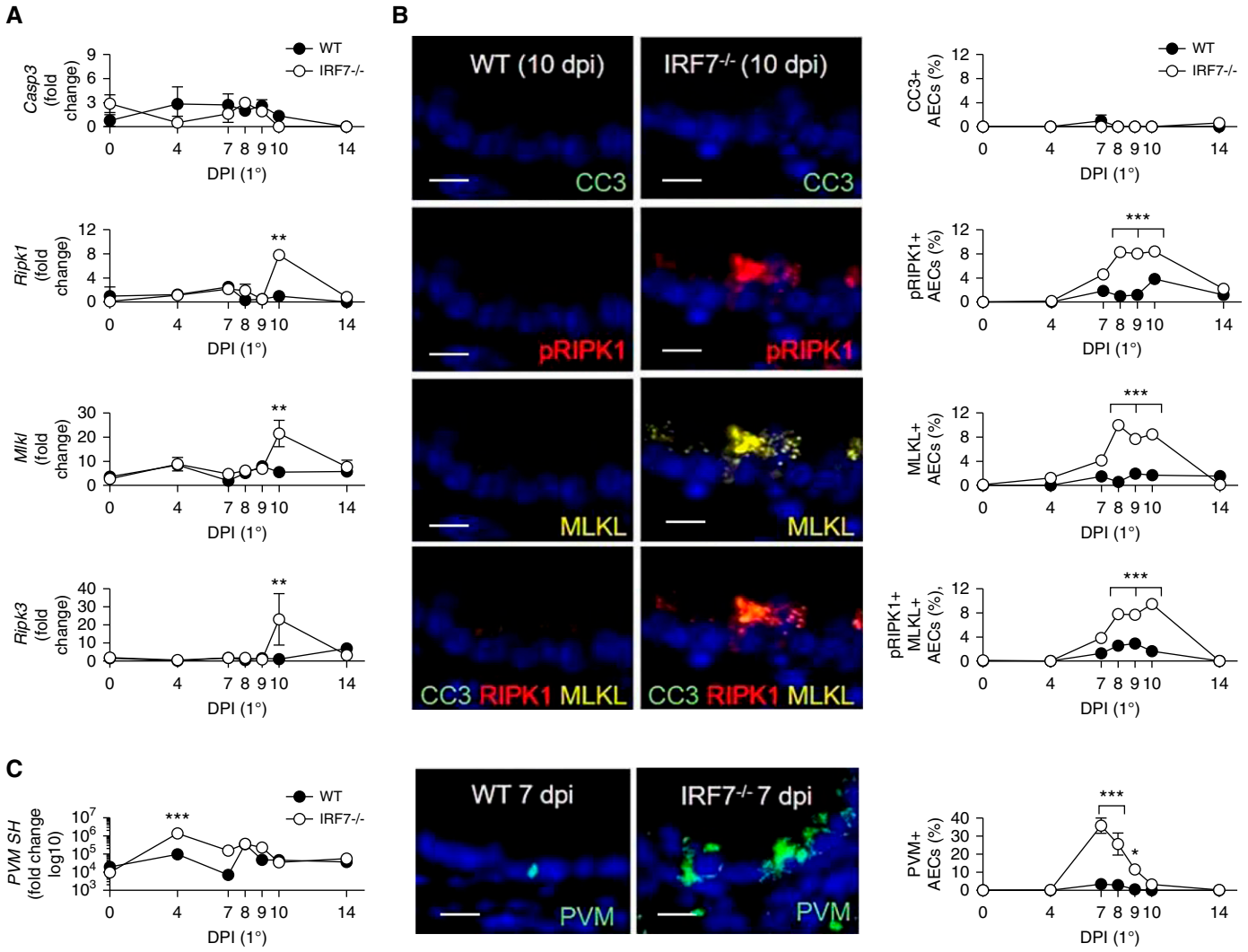

Figure 3. *In vivo Pneumovirus* infection induces necroptotic cell death in the airway epithelium. Neonatal wild-type (WT) and IRF7$^{-/-}$ (IFN regulatory factor 7) mice were infected with pneumonia virus of mice (PVM) (2 plaque-forming units) and cell death–related genes/proteins, and viral load was assessed over time. (*A*) Lung gene expression of *caspase-3*, *Ripk1* (receptor-interacting protein kinase-1), *Mlkl* (mixed lineage kinase domain-like pseudokinase), and *Ripk3*. (*B*) Representative micrographs (×400 magnification; scale bar, 20 μm) of cleaved caspase-3 (CC3) (green), pRIPK1 (phosphorylated RIPK1) (red), and pMLKL (phosphorylated MLKL) (yellow); and quantification of pRIPK1, pMLKL, and CC3 in airway epithelial cells (AECs). (*C*) Lung gene expression of PVM SH gene: representative micrographs (×400 magnification; scale bar, 20 μm) of PVM (green) and quantification of PVM^{+} AECs. Data are representative of $n = 2$ experiments with four to six neonates in each group and are presented as mean ± SEM. Data were analyzed by two-way ANOVA with Sidak's *post hoc* test. $^{*}P < 0.05$, $^{**}P < 0.01$, and $^{***}P < 0.001$ are compared with PVM-infected WT mice at each time point. *Casp3* = *caspase-3*; DPI = days postinfection.

Figure 6E), and airway remodeling (ASM growth, mucus hypersecretion; *see* Figure 6F), further suggesting that necroptosis is pathogenic in the context of RSV bronchiolitis.

Pneumovirus Infection Induces Necroptosis and HMGB1 Release in Differentiated mAECs

To definitively show that PVM induces the release of HMGB1 from AECs in an RIPK1 kinase–dependent manner, we next cultured primary mAECs from WT and RIPK1$^{K45A/K45A}$ Tg mice. Because PVM does not infect undifferentiated mAECs, we differentiated the cells at ALI before inoculation. Consistent with hAECs, *Pneumovirus* infection increased pRIPK1^{+} and MLKL^{+} mAECs, in the absence of a CC3^{+} signal (Figure 7A), and increased dsDNA in the basal media at 24 hpi (*see* Figure 7B). In the absence of RIPK1 kinase activity, pRIPK1^{+} and MLKL^{+} cells were significantly decreased (*see* Figure 7C), as was translocation and release of HMGB1 (*see* Figure 7D). Similarly, treatment of WT mAECs with Nec-1s decreased HMGB1 translocation, and both Nec-1s or GW80 decreased HMGB1 release (*see* Figure 7E). Consistent with the *in vivo* findings, CC3 was elevated in PVM-infected mAECs treated with the MLKL but not the RIPK1 inhibitor (*see* Figure 7F).

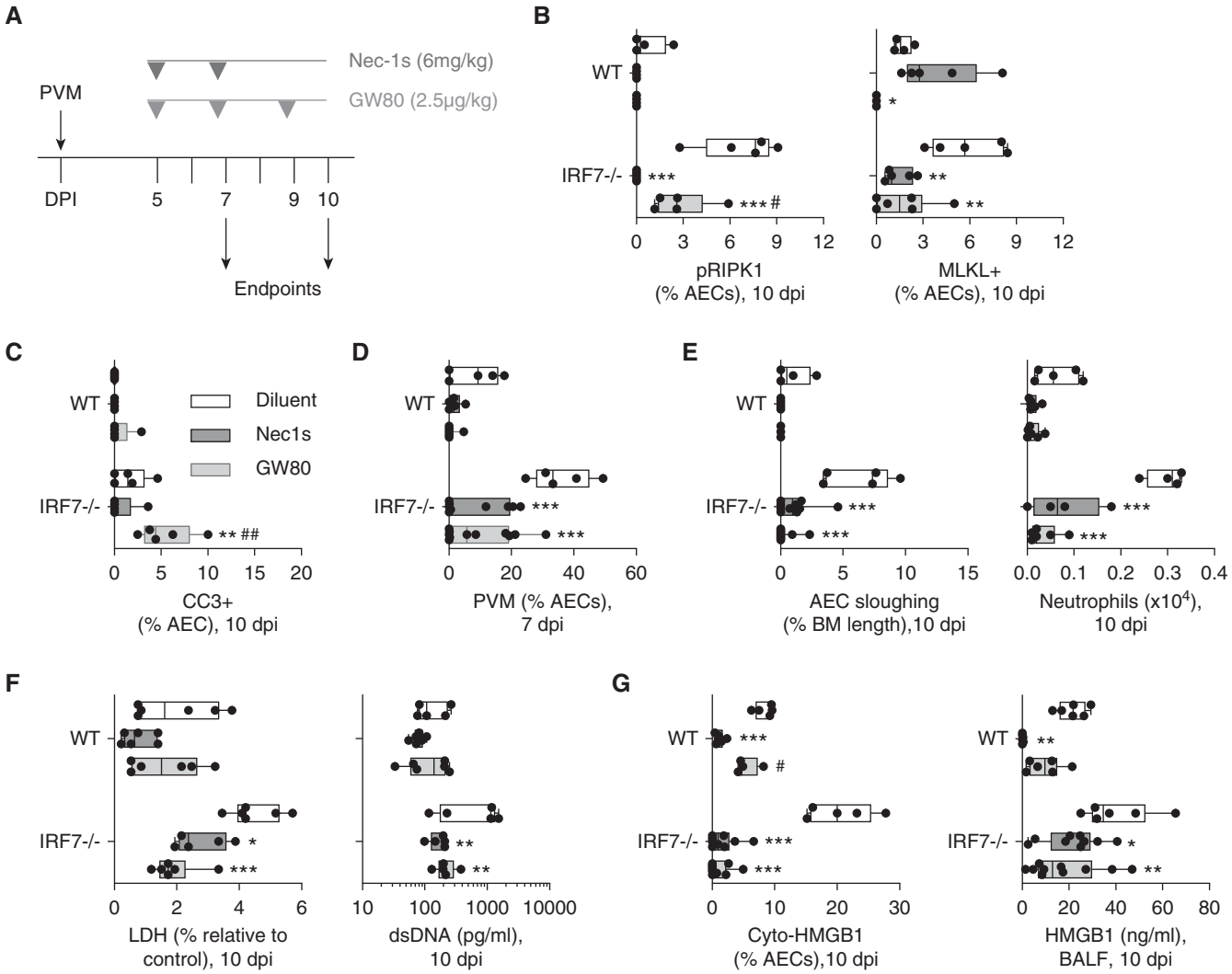

Figure 4. Inhibition of RIPK1 (receptor-interacting protein kinase-1) or pMLKL (phosphorylated mixed lineage kinase domain-like pseudokinase) reduces alarmin release and bronchiolitis in IRF7$^{-/-}$ (IFN regulatory factor 7) mice during acute viral infection. Neonatal wild-type (WT) and IRF7$^{-/-}$ mice were infected with pneumonia virus of mice (PVM) (2 plaque-forming units) at 7 days of age. Mice were treated with either an RIPK1 inhibitor (Necrostatin-1s [Nec-1s]) or MLKL inhibitor (GW80). Alarmin release and bronchiolitis-associated pathologies were assessed at 7 and 10 dpi. (*A*) Study design. (*B*) Quantification of pRIPK1 and MLKL^{+} airway epithelial cells (AECs). (*C*) Quantification of CC3^{+} AECs. (*D*) Quantification of PVM^{+} AECs. (*E*) AEC sloughing normalized to BM length and neutrophils in BAL fluid (BALF). (*F*) Lactate dehydrogenase (LDH) and double-stranded (ds)DNA in BALF. (*G*) Quantification of cyto-HMGB1 (high mobility group box 1) and HMGB1 protein expression in BALF. Data are representative of $n = 2$ experiments with four to six neonates in each group and are presented as box-and-whisker plots showing quartiles (boxes) and range (whiskers). Data were analyzed by two-way ANOVA with Sidak's *post hoc* test. $^{*}P < 0.05$, $^{**}P < 0.01$, and $^{***}P < 0.001$ are compared with untreated (diluent) WT or IRF7$^{-/-}$-infected mice. $^{\#}P < 0.05$ and $^{\#\#}P < 0.01$ are compared with Nec-1s–treated WT or IRF7$^{-/-}$-infected mice. BM = basement membrane; CC3 = cleaved caspase-3; dpi = days postinfection; GW80 = GW806742X; pRIPK1 = phosphorylated RIPK1.

Inhibition of pRIPK1or MLKL during Severe Bronchiolitis Prevents Progression to Later Asthma

Severe or frequent lower respiratory infections are an independent risk factor for asthma (2–4). This epidemiology is captured in our preclinical model because a secondary insult promotes experimental asthma (35). Therefore, we hypothesized that inhibition of *Pneumovirus*-associated necroptosis in early life would prevent the later development of virus-induced or allergen-induced asthma. WT and IRF7$^{-/-}$ mice were infected with PVM in early life and treated with Nec-1s or GW80 in infancy, then, 6 weeks later, challenged with either PVM or exposed to cockroach extract (1/wk for 4 wk) to induce experimental asthma (Figure 8A). Pharmacological inhibition of RIPK1 or MLKL in neonates decreased ASM remodeling, mucus hypersecretion, and eosinophilic inflammation in the predisposed IRF7$^{-/-}$ mice (*see* Figures 8B–8E).

Discussion

New therapies are needed to reduce the significant mortality and morbidity associated with RSV bronchiolitis (1). Here

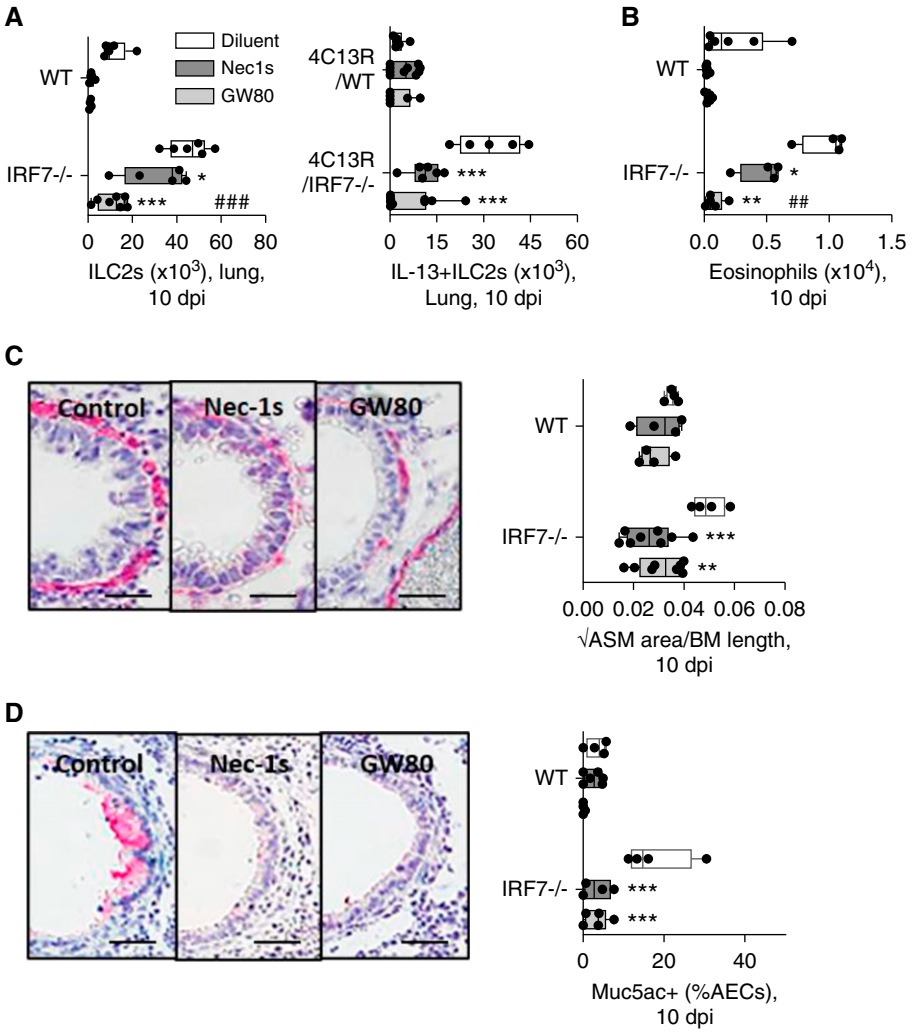

Figure 5. Inhibition of RIPK1 (receptor-interacting protein kinase-1) or MLKL (mixed lineage kinase domain-like pseudokinase) prevents the development of type 2 inflammation. Neonatal wild-type (WT) and IRF7$^{-/-}$ (IFN regulatory factor 7) mice were infected with pneumonia virus of mice (2 plaque-forming units) at 7 days of age. Mice were treated with either an RIPK1 inhibitor (Necrostatin-1s [Nec-1s]) or a MLKL inhibitor (GW80), and markers of type 2 inflammation were assessed at 10 dpi. (*A*) Total IL-13–producing group 2 innate lymphoid cells (ILC2s) in lung. The number of IL-13 + ILC2s in the lung were quantified in 4C13R/WT and 4C13R/IRF7$^{-/-}$-infected mice. (*B*) Eosinophils in BAL fluid. (*C*) Representative micrograph (×100 magnification; scale bar, 50 μm) and quantification of ASM. (*D*) Representative micrograph (×100 magnification; scale bar, 50 μm) and quantification of Muc5ac^{+} AECs. Data are representative of $n = 2$ experiments with four to six neonates in each group and are presented as box-and-whisker plots showing quartiles (boxes) and range (whiskers). Data were analyzed by two-way ANOVA with Sidak's *post hoc* test. $^{*}P < 0.05$, $^{**}P < 0.01$, and $^{***}P < 0.001$ are compared with untreated (diluent) WT or IRF7$^{-/-}$ or 4C13R/WT or 4C13R/IRF7$^{-/-}$-infected mice. $^{\#\#}P < 0.01$ and $^{\#\#\#}P < 0.001$ are compared with Nec-1s–treated WT or IRF7$^{-/-}$-infected mice. AECs = airway epithelial cells; ASM = airway smooth muscle; BM = basement membrane; dpi = days postinfection; GW80 = GW806742X.

we show that infection with human RSV or mouse PVM induces necroptosis in AECs using both *in vivo* and *in vitro* model systems, and that this contributes to disease pathology and pathogenesis. Specifically, we show that inhibition of pRIPK1 kinase activity or MLKL ablates RSV/PVM-associated necroptosis, attenuating the release of the proinflammatory alarmin HMGB1 and downstream sequelae. In addition to improving viral control and ameliorating viral bronchiolitis-associated immunopathology, inhibition of necroptosis in infancy protected against the later development of viral and allergic experimental asthma.

A hallmark of severe viral bronchiolitis is the loss of airway epithelial integrity, leading to epithelial cell sloughing and formation of Creola bodies in the airway lumen (41). However, the mode of cell death has remained elusive. Using cultured hAECs, we and others have shown that RSV infection does not increase caspase-3/7 or caspase-9 activity, markers of apoptotic death (42, 43). This response may reflect the ability of RSV, via nonstructural protein-1 and protein-2, and other molecules, to actively inhibit apoptosis (43–45). Here we confirm that RSV infection fails to induce apoptosis and show for the first time in primary hAECs that RSV induces RIPK1 activation (monitored by autophosphorylation on Ser166) and MLKL-dependent loss of cell viability, indicative of necroptosis. Inhibition of pRIPK1 kinase activity or MLKL decreased cytoplasmic translocation and release of HMGB1, and also decreased viral burden, suggesting that therapies that ablate epithelial necroptosis will exhibit dual antiviral and antiinflammatory activity.

To explore the contribution of necroptosis *in vivo*, we used a neonatal model of severe bronchiolitis that uses low-dose viral infection in a genetically susceptible host (to simulate the gene–environment interactions that underpin disease) (35). Notably, epithelial sloughing, a hallmark feature of bronchiolitis, is absent in mice following inoculation with human RSV, even at supraphysiological doses. This likely reflects the fact that *Pneumoviruses* are host-specific (46, 47). By performing temporal studies, we show in PVM-infected neonatal IRF7$^{-/-}$ mice that necroptosis *1*) is the primary model of AEC death during bronchiolitis, *2*) is initiated soon after peak viral replication, and *3*) precedes the development of airway remodeling and type 2 inflammation. Pharmacologic or genetic ablation of necroptosis decreased AEC sloughing and attenuated the proinflammatory neutrophilic response. This prevented the development of type 2 inflammation and ASM remodeling in infancy, and later development of experimental asthma. This was particularly apparent in mice treated with the MLKL inhibitor, which had a greater impact on eosinophils, compared with RIPK1 inhibition, suggesting either RIPK1 conveys

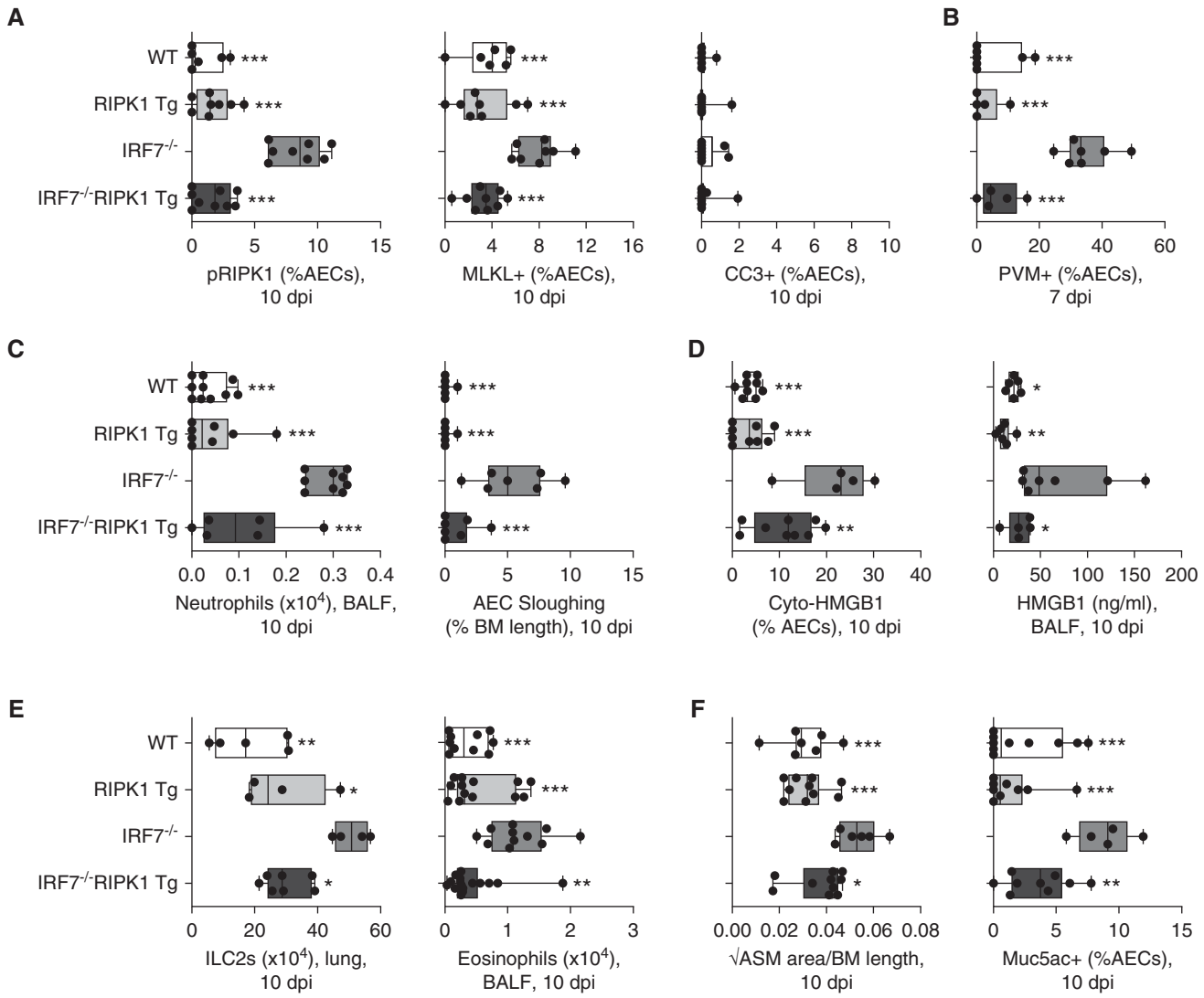

Figure 6. RIPK1 (receptor-interacting protein kinase-1) kinase-dead knockin mice are protected from viral bronchiolitis. Neonatal WT, RIPK1$^{K45A/K45A}$, IRF7$^{-/-}$ (IFN regulatory factor 7), and IRF7$^{-/-}$ RIPK1$^{K45A/K45A}$ mice were infected with pneumonia virus of mice (PVM) (2 plaque-forming units) at 7 days of age. Alarmin release and bronchiolitis-associated pathologies were assessed at 7 and 10 dpi. (*A*) Quantification of pRIPK1, MLKL (mixed lineage kinase domain-like pseudokinase), and CC3^{+} airway epithelial cells (AECs). (*B*) Quantification of PVM. (*C*) Neutrophils in BAL fluid (BALF) and quantification of AEC sloughing. (*D*) Quantification of cytoplasmic HMGB1 (high mobility group box 1) and HMGB1 expression in BALF. (*E*) IL-13–producing group 2 innate lymphoid cells in lung and eosinophils in BALF. (*F*) Quantification of airway smooth muscle area and Muc5ac^{+} AECs. Data are representative of $n = 2$ experiments with four to six neonates in each group and are presented as box-and-whisker plots showing quartiles (boxes) and range (whiskers). Data were analyzed by one-way ANOVA with Dunnett's *post hoc* test. $^{*}P < 0.05$, $^{**}P < 0.01$, and $^{***}P < 0.001$ are compared with IRF7$^{-/-}$-infected mice. ASM = airway smooth muscle; BM = basement membrane; CC3 = cleaved caspase-3; dpi = days postinfection; ILC2s = IL-13–producing group 2 innate lymphoid cells; pRIPK1 = phosphorylated RIPK1; WT = wild-type.

some small protective functions or that MLKL is involved in cell death–independent pathways that promote type 2 inflammation. The impetus for this study stemmed from our unpublished observations demonstrating that HMGB1 is highly pathogenic in the context of bronchiolitis and reports in the literature linking necroptosis to HMGB1 release (12, 37). We show that HMGB1 levels are elevated in nasopharyngeal samples of RSV-infected children and that the beneficial effects of inhibiting necroptosis (*in vivo* in mice and *in vitro* cultured AECs) are associated with a marked decrease in HMGB1 levels. Thus, our findings suggest that inhibiting HMGB1, through monoclonal antibody–mediated neutralization or inhibition of necroptosis, will reduce the high morbidity, and potentially mortality, of severe RSV bronchiolitis. By ablating the onset of type 2 inflammation and ASM remodeling, necroptosis inhibitors may serve as primary preventatives for asthma in predisposed individuals.

In both *in vitro* and *in vivo* models, genetic or pharmacologic inhibition of RIPK1 kinase activity and MLKL decreased viral load. This was unexpected in the

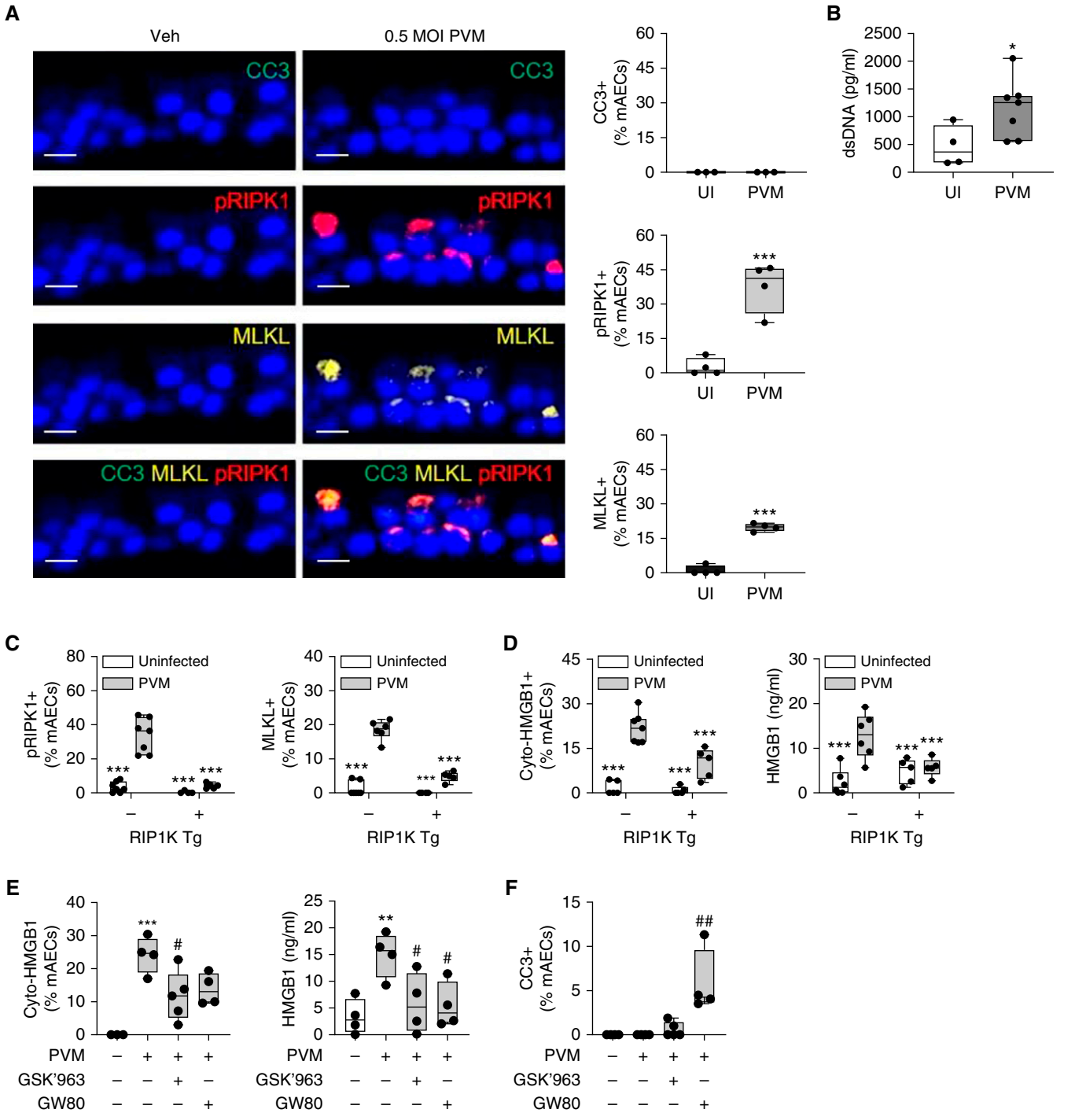

Figure 7. Murine *Pneumovirus* infection induces necroptosis and HMGB1 (high mobility group box 1) release in differentiated mouse airway epithelial cells (mAECs). mAECs were differentiated at air–liquid interface. Cells were infected with pneumonia virus of mice (PVM) and expression of HMGB1 and necroptosis proteins were assessed at 24 hours postinfection. (*A*) Representative images (×400 magnification; scale bar, 20 μm) of cleaved caspase-3 (CC3) (green), pRIPK1 (phosphorylated receptor-interacting protein kinase-1) (red), and MLKL (mixed lineage kinase domain-like pseudokinase) (yellow); and quantification of CC3, pRIPK1, and MLKL^{+} AECs. (*B*) Double-stranded (ds)DNA expression in basal media. (*C*) Quantification of pRIPK1 and MLKL^{+} AECs. (*D*) Quantification of cyto-HMGB1^{+} AECs. HMGB1 protein expression in basal media. (*E*) Quantification of cyto-HMGB1^{+} AECs. HMGB1 protein expression in basal media. (*F*) Quantification of CC3^{+} AECs. Data are representative of $n = 2$ experiments with four to seven neonates in each group and are presented as box-and-whisker plots showing quartiles (boxes) and range (whiskers). (*A*–*F*) Data were analyzed using Student's *t* test (*A* and *B*), two-way ANOVA with Sidak's *post hoc* test (*C* and *D*), or one-way ANOVA with Dunnett *post hoc* test (*E* and *F*). (*A*–*F*) $^{*}P < 0.05$, $^{**}P < 0.01$, and $^{***}P < 0.001$ are compared with uninfected mAECs (*A*, *B*, *E*, *F*) or PVM-infected RIPK1$^{K45A/K45A}$ mAECs (*C* and *D*). $^{\#}P < 0.05$ and $^{\#\#}P < 0.01$ are compared with PVM-infected wild-type mAECs. GW80 = GW806742X; MOI = multiplicity of infection; Tg = transgenic; UI = uninfected; Veh = vehicle.

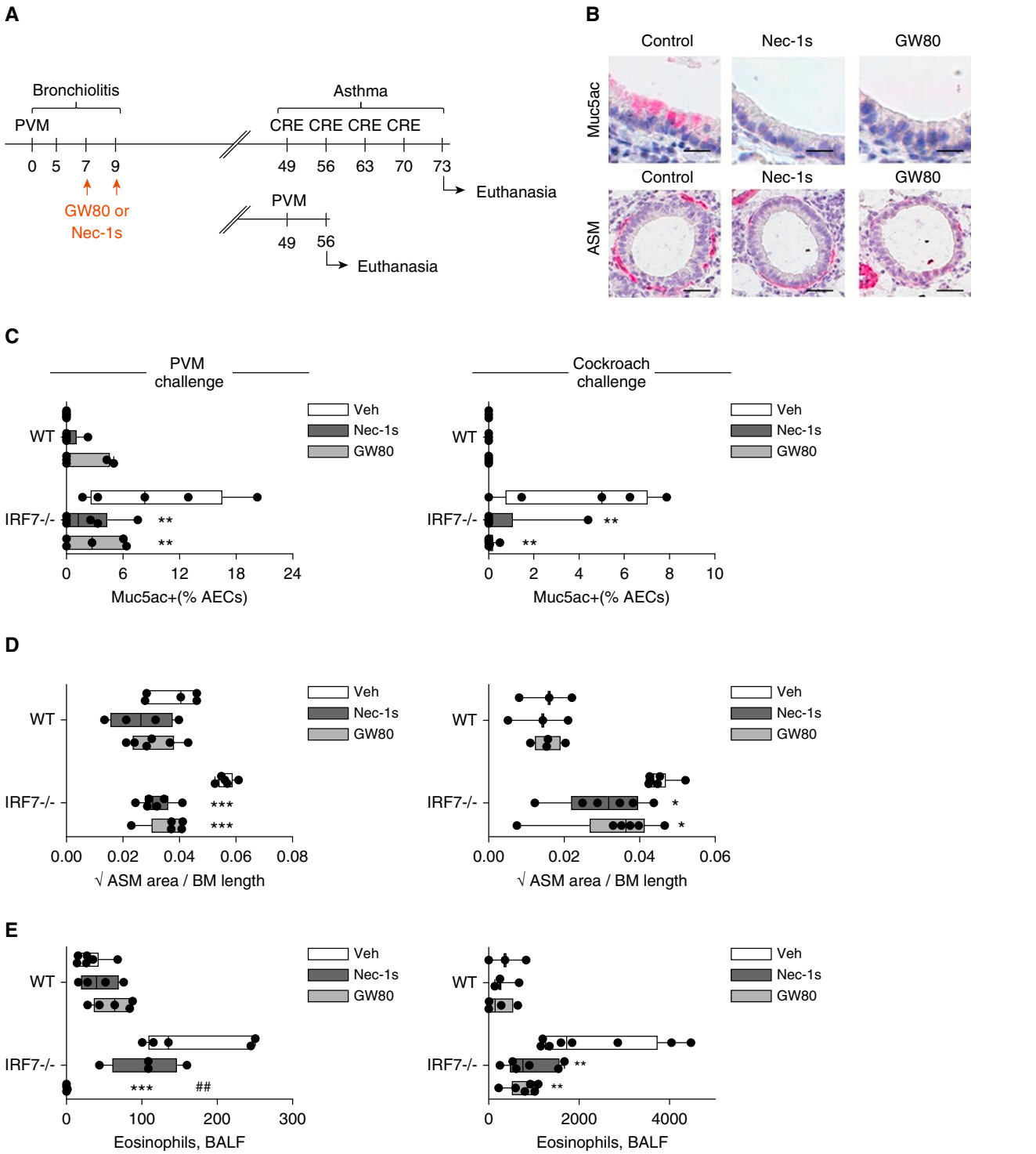

Figure 8. Inhibition of pRIPK1 (phosphorylated receptor-interacting protein kinase-1) or MLKL (mixed lineage kinase domain-like pseudokinase) during severe bronchiolitis prevents progression to later asthma. (*A*) Study design. (*B*) Representative micrograph of Muc5ac (red; ×200 magnification; scale bar, 25 μm) and airway smooth muscle (ASM) staining (red; ×100 magnification; scale bar, 50 μm) in pneumonia virus of mice (PVM)/PVM-infected IRF7$^{-/-}$ mice. (*C*) Quantification of Muc5ac^{+} cells. (*D*) Quantification of ASM area. (*E*) Eosinophils in BALF. (*C–E*) Neonatal wild-type (WT) and IRF7$^{-/-}$ (IFN regulatory factor 7) mice were infected with PVM (2 plaque-forming units), treated with the RIPK1 (Necrostatin-1s [Nec-1s]) or MLKL inhibitor (GW80), then challenged with PVM (left-hand panels in *C–E*) or cockroach allergen (right-hand panels in *C–E*) in later life. Data are representative of $n = 2$ experiments with three to six neonates in each group and are presented as box-and-whisker plots showing quartiles (boxes) and range (whiskers). Data were analyzed using two-way ANOVA with Sidak's *post hoc* test. $^{*}P < 0.05$, $^{**}P < 0.01$, and $^{***}P < 0.001$ are compared with untreated (diluent) WT or IRF7$^{-/-}$-infected mice. $^{\#\#}P < 0.01$ is compared with Nec-1s–treated WT or IRF7$^{-/-}$-infected mice. AECs = airway epithelial cells; BALF = BAL fluid; BM = basement membrane; CRE = cockroach allergen extract; GW80 = GW806742X; Veh = vehicle.

in vivo model because the increase in pRIPK1/MLKL at 7 dpi was not statistically significant. However, it is apparent from the time-course studies that the upregulation and phosphorylation of necroptosis-associated proteins is initiated between 4 and 7 dpi, followed by a sharp increase at 8 to 10 dpi, inferring a feed-forward loop. In other investigations of necroptosis-associated kinases, RIPK3 was shown to limit the propagation of herpes simplex virus, influenza virus A, and vaccinia virus (17, 48, 49); although, notably, this phenotype was not observed with influenza H7H9 infection (50). RIPK3 can contribute to both apoptosis and necroptosis, and is involved in proinflammatory cytokine production, complicating interpretations. As such, even though its expression was increased in PVM-infected mice, we did not seek to assess the role of RIPK3 in the present study. Unlike RIPK3 deficiency, genetic deletion of MLKL did not affect influenza virus A replication or clearance (48). In summary, the consequence of necroptosis on viral pathogenesis appears to be context-dependent and virus-dependent; the latter potentially relating to the ability of the virus to preferentially inhibit or induce apoptosis and/or necroptosis.

The mechanism by which inhibition of necroptosis lowered *Pneumovirus* load remains elusive. In both the *in vivo* and *in vitro* models, inhibition of necroptosis did not lead to an increase in the expression of type I or type III IFNs. However, inhibition of MLKL led to a significant increase in the number of active caspase-3 immunoreactive epithelial cells, despite two different MLKL inhibitors being used. This highly reproducible phenotype was not apparent after RIPK1 inhibition, suggesting that the inhibition of MLKL initiates an RIPK1-dependent apoptotic pathway. The propensity for necroptosis over apoptosis following *Pneumovirus* infection suggests that the virus subverts apoptosis, which is well established. Our findings suggest that blocking necroptosis either overcomes this subversion or initiates a different pathway to apoptosis that is not inhibited by the virus. Further studies are needed to reveal these molecular processes; however, we were able to implicate both intrinsic and extrinsic apoptosis pathways because dual inhibition of caspase-8 and caspase-9 prevented processing of caspase-3 and the fall in viral load induced via MLKL inhibition.

Typically, the induction of necroptosis is achieved by sensitizing cells via the use of a chemical agent and, consequently, such studies are less physiologically relevant. A strength of this study is that RSV/PVM naturally induced necroptosis without the use of an apoptosis inhibitor, likely due to the anticaspase activity of the virus or ablation of a necroptosis repressor. Multiple proinflammatory pathways can induce necroptosis upon viral infection, including TLR (Toll-like receptor) IFN, or TNF receptor activation (13, 14, 18). A limitation of the current study is that we did not explore this specifically; however, the elevated viral load, in the absence of increased IFNs or TNF at 7 or 8 dpi, implicates a virus-sensing pattern recognition receptor.

Conclusions

We demonstrate that in their host-specific setting, *Pneumoviruses* induce necroptosis in AECs, leading to release of HMGB1. Inhibition of RIPK1 kinase activity or MLKL ameliorates the severity of bronchiolitis by decreasing viral load and immunopathology, which in turn prevents the development of type 2 inflammation and associated ASM remodeling. Consequently, susceptibility to later asthma is lowered. Our findings implicate necroptosis in the pathogenesis of bronchiolitis and suggest that therapeutic targeting of its effector kinases would ameliorate bronchiolitis severity and potentially act as an asthma preventative in a subpopulation of individuals whose etiology is linked to early-life viral infections. Further work is required to identify safe and effective ways to target this important pathway, a critical step in developing future RSV therapies. ■

Author disclosures are available with the text of this article at www.atsjournals.org.

References

1. Nair H, Simões EA, Rudan I, Gessner BD, Azziz-Baumgartner E, Zhang JSF, *et al*.; Severe Acute Lower Respiratory Infections Working Group. Global and regional burden of hospital admissions for severe acute lower respiratory infections in young children in 2010: a systematic analysis. *Lancet* 2013;381:1380–1390.
2. Feldman AS, He Y, Moore ML, Hershenson MB, Hartert TV. Toward primary prevention of asthma: reviewing the evidence for early-life respiratory viral infections as modifiable risk factors to prevent childhood asthma. *Am J Respir Crit Care Med* 2015; 191:34–44.
3. Singh AM, Moore PE, Gern JE, Lemanske RF Jr, Hartert TV. Bronchiolitis to asthma: a review and call for studies of gene-virus interactions in asthma causation. *Am J Respir Crit Care Med* 2007;175:108–119.
4. Toivonen L, Forsstrom V, Waris M, Peltola V. Acute respiratory infections in early childhood and risk of asthma at age 7 years. *J Allergy Clin Immunol* 2019;143:407–410, e6.
5. Everard ML, Swarbrick A, Wrightham M, McIntyre J, Dunkley C, James PD, *et al*. Analysis of cells obtained by bronchial lavage of infants with respiratory syncytial virus infection. *Arch Dis Child* 1994;71: 428–432.
6. Johnson JE, Gonzales RA, Olson SJ, Wright PF, Graham BS. The histopathology of fatal untreated human respiratory syncytial virus infection. *Mod Pathol* 2007;20:108–119.
7. Aherne W, Bird T, Court SD, Gardner PS, McQuillin J. Pathological changes in virus infections of the lower respiratory tract in children. *J Clin Pathol* 1970;23:7–18.
8. Stetson DB, Medzhitov R. Type I interferons in host defense. *Immunity* 2006;25:373–381.
9. De Cosmi V, Mehta NM, Boccazzi A, Milani GP, Esposito S, Bedogni G, *et al*. Nutritional status, metabolic state and nutrient intake in children with bronchiolitis. *Int J Food Sci Nutr* 2017;68:378–383.
10. Janssen R, Bont L, Siezen CL, Hodemaekers HM, Ermers MJ, Doornbos G, *et al*. Genetic susceptibility to respiratory syncytial virus bronchiolitis is predominantly associated with innate immune genes. *J Infect Dis* 2007;196:826–834.
11. Siezen CL, Bont L, Hodemaekers HM, Ermers MJ, Doornbos G, Van't Slot R, *et al*. Genetic susceptibility to respiratory syncytial virus bronchiolitis in preterm children is associated with airway remodeling genes and innate immune genes. *Pediatr Infect Dis J* 2009;28: 333–335.
12. Qing DY, Conegliano D, Shashaty MG, Seo J, Reilly JP, Worthen GS, *et al*. Red blood cells induce necroptosis of lung endothelial cells and increase susceptibility to lung inflammation. *Am J Respir Crit Care Med* 2014;190:1243–1254.
13. Robinson N, McComb S, Mulligan R, Dudani R, Krishnan L, Sad S. Type I interferon induces necroptosis in macrophages during infection with Salmonella enterica serovar Typhimurium. *Nat Immunol* 2012;13:954–962.

14. Vanlangenakker N, Bertrand MJ, Bogaert P, Vandenabeele P, Vanden Berghe T. TNF-induced necroptosis in L929 cells is tightly regulated by multiple TNFR1 complex I and II members. *Cell Death Dis* 2011;2: e230.
15. Bell CW, Jiang W, Reich CF III, Pisetsky DS. The extracellular release of HMGB1 during apoptotic cell death. *Am J Physiol Cell Physiol* 2006; 291:C1318–C1325.
16. Vandenabeele P, Galluzzi L, Vanden Berghe T, Kroemer G. Molecular mechanisms of necroptosis: an ordered cellular explosion. *Nat Rev Mol Cell Biol* 2010;11:700–714.
17. Cho YS, Challa S, Moquin D, Genga R, Ray TD, Guildford M, *et al*. Phosphorylation-driven assembly of the RIP1-RIP3 complex regulates programmed necrosis and virus-induced inflammation. *Cell* 2009;137:1112–1123.
18. Takemura R, Takaki H, Okada S, Shime H, Akazawa T, Oshiumi H, *et al*. PolyI:C-induced, TLR3/RIP3-dependent necroptosis backs up immune effector-mediated tumor elimination *in vivo*. *Cancer Immunol Res* 2015;3:902–914.
19. Gaba A, Xu F, Lu Y, Park HS, Liu G, Zhou Y. The Ns1 protein of influenza a virus participates in necroptosis by interacting with Mlkl and increasing its oligomerization and membrane translocation. *J Virol* 2019;93:e01835-18.
20. Spann KM, Baturcam E, Schagen J, Jones C, Straub CP, Preston FM, *et al*. Viral and host factors determine innate immune responses in airway epithelial cells from children with wheeze and atopy. *Thorax* 2014;69:918–925.
21. Werder RB, Lynch JP, Simpson JC, Zhang V, Hodge NH, Poh M, *et al*. PGD2/DP2 receptor activation promotes severe viral bronchiolitis by suppressing IFN-λ production. *Sci Transl Med* 2018;10:eaao0052.
22. Schagen J, Sly PD, Fantino E. Characterizing well-differentiated culture of primary human nasal epithelial cells for use in wound healing assays. *Lab Invest* 2018;98:1478–1486.
23. Takahashi N, Duprez L, Grootjans S, Cauwels A, Nerinckx W, DuHadaway JB, *et al*. Necrostatin-1 analogues: critical issues on the specificity, activity and *in vivo* use in experimental disease models. *Cell Death Dis* 2012;3:e437.
24. Kitur K, Parker D, Nieto P, Ahn DS, Cohen TS, Chung S, *et al*. Toxin-induced necroptosis is a major mechanism of Staphylococcus aureus lung damage. *PLoS Pathog* 2015;11:e1004820.
25. Rock JR, Onaitis MW, Rawlins EL, Lu Y, Clark CP, Xue Y, *et al*. Basal cells as stem cells of the mouse trachea and human airway epithelium. *Proc Natl Acad Sci USA* 2009;106:12771–12775.
26. Hildebrand JM, Tanzer MC, Lucet IS, Young SN, Spall SK, Sharma P, *et al*. Activation of the pseudokinase MLKL unleashes the four-helix bundle domain to induce membrane localization and necroptotic cell death. *Proc Natl Acad Sci USA* 2014;111:15072–15077.
27. Berger SB, Harris P, Nagilla R, Kasparcova V, Hoffman S, Swift B, *et al*. Characterization of GSK'963: a structurally distinct, potent and selective inhibitor of RIP1 kinase. *Cell Death Discov* 2015;1:15009.
28. Lynch JP, Werder RB, Simpson J, Loh Z, Zhang V, Haque A, *et al*. Aeroallergen-induced IL-33 predisposes to respiratory virus-induced asthma by dampening antiviral immunity. *J Allergy Clin Immunol* 2016;138:1326–1337.
29. Rochon J, Gondan M, Kieser M. To test or not to test: preliminary assessment of normality when comparing two independent samples. *BMC Med Res Methodol* 2012;12:81.
30. Hosakote YM, Brasier AR, Casola A, Garofalo RP, Kurosky A. Respiratory syncytial virus infection triggers epithelial HMGB1 release as a damage-associated molecular pattern promoting a monocytic inflammatory response. *J Virol* 2016;90: 9618–9631.
31. Arshad MI, Piquet-Pellorce C, Filliol A, L'Helgoualc'h A, Lucas-Clerc C, Jouan-Lanhouet S, *et al*. The chemical inhibitors of cellular death, PJ34 and Necrostatin-1, down-regulate IL-33 expression in liver. *J Mol Med (Berl)* 2015;93:867–878.
32. Petrie EJ, Hildebrand JM, Murphy JM. Insane in the membrane: a structural perspective of MLKL function in necroptosis. *Immunol Cell Biol* 2017;95:152–159.
33. Simpson J, Lynch JP, Loh Z, Zhang V, Werder RB, Spann K, *et al*. The absence of Interferon-β promotor stimulator-1 (IPS-1) predisposes to bronchiolitis and asthma-like pathology in response to pneumoviral infection in mice. *Sci Rep* 2017;7:2353.
34. Kaiko GE, Phipps S, Angkasekwinai P, Dong C, Foster PS. NK cell deficiency predisposes to viral-induced Th2-type allergic inflammation via epithelial-derived IL-25. *J Immunol* 2010;185: 4681–4690.
35. Lynch JP, Werder RB, Loh Z, Sikder MAA, Curren B, Zhang V, *et al*. Plasmacytoid dendritic cells protect from viral bronchiolitis and asthma through semaphorin 4a-mediated T reg expansion. *J Exp Med* 2018;215:537–557.
36. Kaiko GE, Loh Z, Spann K, Lynch JP, Lalwani A, Zheng Z, *et al*. Toll-like receptor 7 gene deficiency and early-life *Pneumovirus* infection interact to predispose toward the development of asthma-like pathology in mice. *J Allergy Clin Immunol* 2013;131:1331–1339, e10.
37. Mizumura K, Cloonan SM, Nakahira K, Bhashyam AR, Cervo M, Kitada T, *et al*. Mitophagy-dependent necroptosis contributes to the pathogenesis of COPD. *J Clin Invest* 2014;124:3987–4003.
38. Cai Z, Jitkaew S, Zhao J, Chiang HC, Choksi S, Liu J, *et al*. Plasma membrane translocation of trimerized MLKL protein is required for TNF-induced necroptosis. *Nat Cell Biol* 2014;16:55–65.
39. Weng D, Marty-Roix R, Ganesan S, Proulx MK, Vladimer GI, Kaiser WJ, *et al*. Caspase-8 and RIP kinases regulate bacteria-induced innate immune responses and cell death. *Proc Natl Acad Sci USA* 2014; 111:7391–7396.
40. Berger SB, Kasparcova V, Hoffman S, Swift B, Dare L, Schaeffer M, *et al*. Cutting Edge: RIP1 kinase activity is dispensable for normal development but is a key regulator of inflammation in SHARPIN-deficient mice. *J Immunol* 2014;192:5476–5480.
41. Visscher DW, Myers JL. Bronchiolitis: the pathologist's perspective. *Proc Am Thorac Soc* 2006;3:41–47.
42. Baturcam E, Snape N, Yeo TH, Schagen J, Thomas E, Logan J, *et al*. Human metapneumovirus impairs apoptosis of nasal epithelial cells in asthma via HSP70. *J Innate Immun* 2017;9:52–64.
43. Thomas KW, Monick MM, Staber JM, Yarovinsky T, Carter AB, Hunninghake GW. Respiratory syncytial virus inhibits apoptosis and induces NF-kappa B activity through a phosphatidylinositol 3-kinase-dependent pathway. *J Biol Chem* 2002;277:492–501.
44. Bitko V, Shulyayeva O, Mazumder B, Musiyenko A, Ramaswamy M, Look DC, *et al*. Nonstructural proteins of respiratory syncytial virus suppress premature apoptosis by an NF-kappaB-dependent, interferon-independent mechanism and facilitate virus growth. *J Virol* 2007;81:1786–1795.
45. Groskreutz DJ, Monick MM, Yarovinsky TO, Powers LS, Quelle DE, Varga SM, *et al*. Respiratory syncytial virus decreases p53 protein to prolong survival of airway epithelial cells. *J Immunol* 2007;179:2741–2747.
46. Bem RA, Domachowske JB, Rosenberg HF. Animal models of human respiratory syncytial virus disease. *Am J Physiol Lung Cell Mol Physiol* 2011;301:L148–L156.
47. Schmidt ME, Oomens AGP, Varga SM. Single-cycle respiratory syncytial virus infection induces robust adaptive immune responses and reduces disease severity in mice. *J Immunol* 2018;200:60.62.
48. Nogusa S, Thapa RJ, Dillon CP, Liedmann S, Oguin TH III, Ingram JP, *et al*. RIPK3 activates parallel pathways of MLKL-driven necroptosis and FADD-mediated apoptosis to protect against influenza A virus. *Cell Host Microbe* 2016;20:13–24.
49. Huang Z, Wu SQ, Liang Y, Zhou X, Chen W, Li L, *et al*. RIP1/RIP3 binding to HSV-1 ICP6 initiates necroptosis to restrict virus propagation in mice. *Cell Host Microbe* 2015;17:229–242.
50. Xu YL, Tang HL, Peng HR, Zhao P, Qi ZT, Wang W. RIP3 deficiency ameliorates inflammatory response in mice infected with influenza H7N9 virus infection. *Oncotarget* 2017;8:27715–27724.